Seasat Synthetic Aperture Radar: Ocean Wave Detection Capabilities

Abstract. *A preliminary assessment has been made of the capability of the Seasat synthetic aperture radar to detect ocean waves. Comparison with surface and aircraft measurements from five passes of the satellite over the Gulf of Alaska indicates agreement to within about ± 15 percent in wavelength and about ± 25° in wave direction. These results apply to waves 100 to 250 meters in length, propagating in a direction predominantly across the satellite track, in sea states with significant wave height* ($H_{1/3}$) *in a range of 2 to 3.5 meters.*

It has been recognized for some time that airborne imaging radars can provide useful ocean wave information, although the exact mechanism by which microwave radar energy is backscattered and modulated to produce ocean wave imagery is still not well understood (*1*, *2*). This study is the first assessment of the ocean wave detection capabilities of the Seasat synthetic aperture radar (SAR). SAR data from five Gulf of Alaska Seasat Experiment (GOASEX) revolutions were provided by the Jet Propulsion Laboratory (JPL) in the form of positive transparencies.

The imagery available for this study was the product of uncontrolled processing; it was intended to be used only for a preliminary evaluation. The characteristics of this imagery were as follows. Range (across the satellite track) and azimuth (along the satellite track) resolution varied from 30 to 50 m. Azimuth scale factors varied by 2 to 10 percent, and range scale factors varied by as much as 17 percent in each of four subswaths of a given revolution. The distributed target dynamic range was about 13 dB for revolutions 1126 and 1169 and 16 dB for revolutions 1255, 1269, and 1306, but there was an additional 5- to 10-dB variation from near to far range because of mispositioning of the sensitivity time control gain adjustments in the SAR. Time coding errors may be as high as 5 seconds, so that specification of geographical location in imagery without land references may be in error by as much as 25 km. Despite these shortcomings in this preliminary version of the SAR imagery, the data yielded useful ocean wave information for comparison with surface and aircraft measurements.

Optical Fourier transforms (OFT's) of SAR ocean scenes yielded intensity spectra of the type shown in Fig. 1 (*3*). The wavelengths of linear features in the imagery are inversely proportional to distance from the OFT center, and the wave direction relative to the spacecraft heading (azimuth) is measured positive clockwise from the horizontal. The OFT process produces two peaks for each dominant wavelength present in the imagery, thus creating a 180° ambiguity in the wave direction. In this study, we have tentatively resolved the ambiguity by choosing either that direction which best agrees with available surface measurements or that direction which propagates waves from the open ocean toward shore. A rigorous resolution of this ambiguity in wave direction can be achieved by focusing the image on an optical processor (*2*). For details of the OFT techniques used in this study, see Born *et al.* (*4*).

Reduction of the OFT data included corrections for the range scale variations

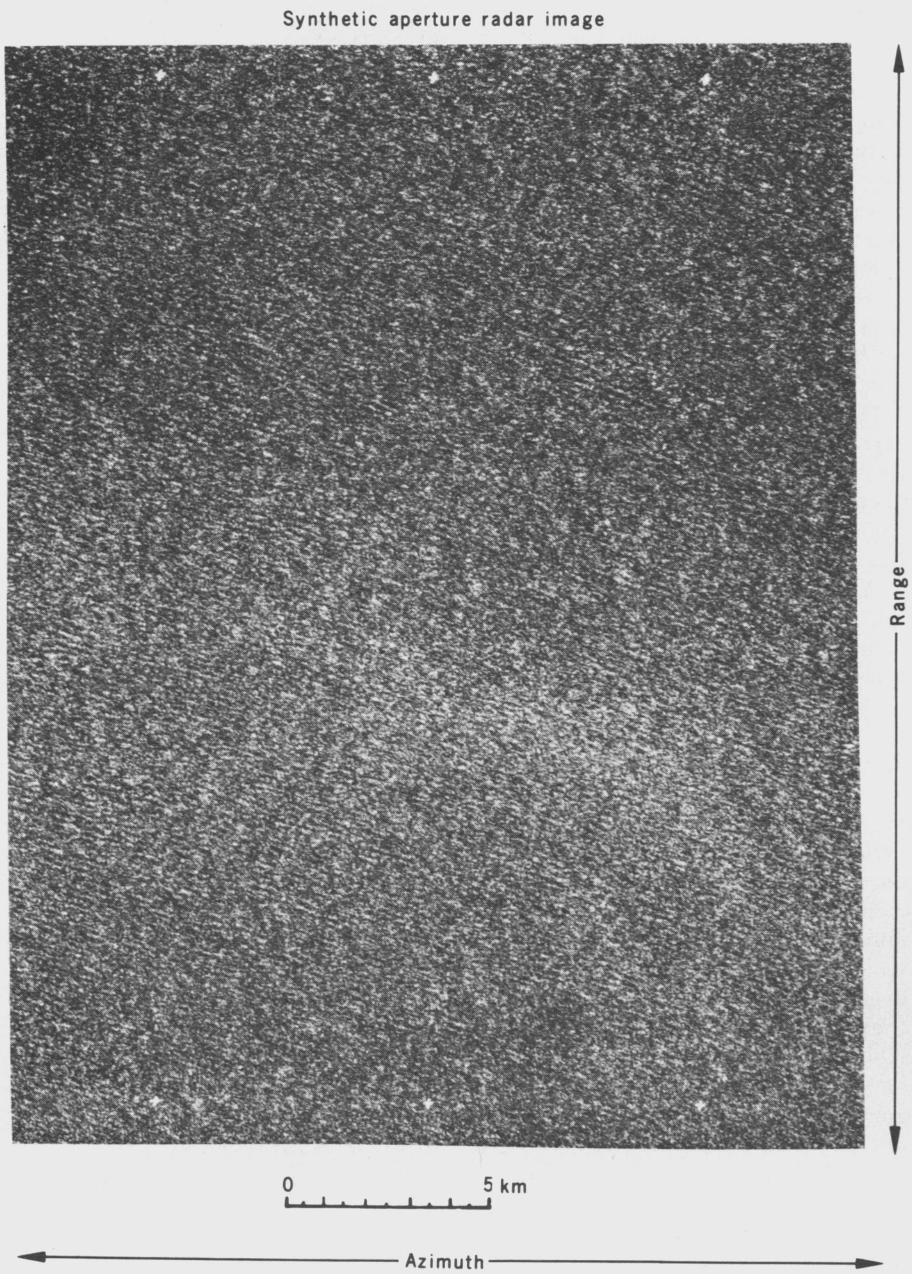

Fig. 1. Seasat SAR image and the resulting optical Fourier transform.

0036-8075/79/0629-1418$00.75/0

mentioned above. Inaccuracies associated with the somewhat subjective determination of the position of the OFT intensity peaks are the principal sources of errors, and these errors vary significantly with each particular spectrum. A rigorous error analysis of the technique has not yet been made, but successive measurements of the same OFT by different individuals have suggested a repeatability of about ± 15 percent in wavelength and ± 20° in wave direction.

Wavelengths and wave directions derived from the OFT measurements were compared with surface and aircraft measurements obtained coincidentally with the acquisition of the Seasat SAR imagery. The principal source of the surface truth was a pitch-roll (P-R) buoy, developed by the National Institute of Oceanography in Wormley, England. The buoy, deployed from the National Oceanic and Atmospheric Administration (NOAA) research vessel *Oceanographer*, measured vertical acceleration, pitch, roll angles, and orientation relative to north. Cross-correlations of these signals yielded a decomposition of the variance of the sea surface over frequency and direction (*5*). An integration over all directions then yielded one-dimensional frequency spectra, the peak frequency of which was inserted into the small-amplitude, linear gravity wave dispersion relationship to obtain the dominant wavelength present. In a more rigorous approach one would transform the entire frequency spectra into wavelength spectra; the resulting peak wavelength is then compared with the OFT measurements (*6*). The spectral peaks examined in the study were sufficiently sharp to justify the present approach, although the transformations are planned as part of a later analysis. The sampling rate of the buoy was 2 Hz, and the nominal operating time was 30 minutes (bracketing the time of the satellite overpass). The spectra were resolved into 64 frequency bands, each of approximately 64 degrees of freedom; this translates roughly into accuracies of about ± 10° for wave direction and ± 20 percent for wavelengths in the range of interest.

Similarly, the peaks of one-dimensional frequency spectra, computed from accelerometer measurements made by NOAA National Data Buoy Office (NDBO) data buoys, yielded dominant wavelength estimates that were also compared with Seasat SAR data. Because of the finer frequency resolution of these buoys, somewhat smaller errors (about ± 15 percent in wavelength) are estimated for the range of interest.

Finally, for three of the five revolutions examined, the Canadian CV-580 aircraft, equipped with the dual-polarized X- and L-band SAR of the Environmental Research Institute of Michigan (ERIM) provided ocean surface imagery for comparison with Seasat SAR. Direct measurements were made of the wavelength and wave direction of ocean wave patterns in the raw imagery; a conversion was made from slant to ground-range coordinates, and Doppler corrections were also applied to compensate for aircraft motion (*7*). The errors associated with this procedure were estimated to be about ± 10 m in wavelength and about ± 10° in wave direction.

Tables 1 through 3 present a summary of the resulting Seasat and surface or aircraft data pairs compared in this study. Two important limitations of the data set are apparent. Surface measurements indicate that (i) most waves present in the imagery examined thus far were traveling toward the east in a narrow range of directions and (ii) significant wave heights ($H_{1/3}$) were limited to a range of about 1 to 3.5 m.

Table 1. Seasat data taken within 100-km coincidence of surface or aircraft data (Table 2); λ, wavelength; θ, wave direction; subscripts T and A refer to direction measurements made relative to true north and azimuth direction, respectively.

Date (1978)	Revolution	Data source	Time (G.M.T.)	Location		Sea state data		
				Subswath	Distance from swath start (km)	λ (m)	θ_T (deg)	θ_A (deg)
9/13	1126A	ERIM OFT	17:29	4	315	194	096/276	125
9/13	1126A	ERIM OFT	17:29	4	475	217	097/277	126
9/13	1126A	ERIM OFT	17:30	4	695	205	083/263	113/293
9/13	1126A	ERIM OFT	17:30	4	695	265	114/294	144/324
9/13	1126A	JPL OFT	17:30	1	725	225	097/277	127/307
9/13	1126A	JPL OFT	17:30	1	725	259	077/257	107/287
9/16	1169A	ERIM OFT	17:43	1	810	329	094/274	122
9/16	1169A	ERIM OFT	17:45	1	1445	260	090	120
9/16	1169A	ERIM OFT	17:45	2	1445	231	083	113
9/16	1169A	ERIM OFT	17:45	3	1445	252	088	118
9/16	1169A	JPL OFT	17:45	2	1460	215	091	121
9/16	1169A	JPL OFT	17:45	1	1500	289	104	135
9/22	1255A	ERIM OFT	18:09	2	870	212	100	130
9/22	1255A	JPL OFT	18:09	2	930	188	089	119
9/22	1255A	ERIM OFT	18:09	2	935	182	084	114
9/22	1255A	ERIM OFT	18:09	2	1000	191	090	121
9/22	1255A	ERIM OFT	18:09	2	1035	181	087	118
9/22	1255A	ERIM OFT	18:09	2	870	212	100	130
9/22	1255A	JPL OFT	18:09	2	930	188	089	119
9/22	1255A	ERIM OFT	18:09	2	935	182	084	114
9/22	1255A	ERIM OFT	18:09	2	1000	191	090	121
9/22	1255A	ERIM OFT	18:09	2	1035	181	087	118
9/23	1269A	ERIM OFT	17:51	(Swiftsure Bank)		165	091	121
9/23	1269A	ERIM OFT	17:51	(Swiftsure Bank)		165	091	121
9/23	1269A							
9/26	1306D	ERIM OFT	08:00	(Swiftsure Bank)		Spectra not discernible		
9/26	1306D	ERIM OFT	08:00	(Swiftsure Bank)		Spectra not discernible		
9/26	1306D	ERIM OFT	08:00	(Swiftsure Bank)		Spectra not discernible		
9/26	1306D	ERIM OFT	08:00	(Swiftsure Bank)		Spectra not discernible		
9/26	1306D							

Table 2. Surface and aircraft data (surface truth data) taken within 100-km coincidence of Seasat measurements (Table 1); λ, wavelength; θ, wave direction; U, wind speed; α, wind direction. Subscripts T and A are the same as in Table 1.

Date (1978)	Revolution	Data source	Time (G.M.T.)	Location: Subswath	Location: Distance from swath start (km)	Sea state data: λ (m)	Sea state data: θ_T (deg)	Sea state data: θ_A (deg)	Sea state data: $H_{1/3}$ (m)	Wind data: U (m/sec)	Wind data: α_T (deg)	Wind data: α_A (deg)
9/13	1126A	NDBO 05	17:44–18:16	4	385	193			2.1	7.4	331	000
9/13	1126A	NDBO 05	17:44–18:16	4	385	193			2.1	7.4	331	000
9/13	1126A	P-R buoy	17:29–18:04	2	730	256	096/276	126/306	2.7	3.8	244	274
9/13	1126A	P-R buoy	17:29–18:04	2	730	256	096/276	126/306	2.7	3.8	244	274
9/13	1126A	P-R buoy	17:29–18:04	2	730	256	096/276	126/306	2.7	3.8	244	274
9/13	1126A	P-R buoy	17:29–18:04	2	730	256	096/276	126/306	2.7	3.8	244	274
9/16	1169A	NDBO 02	17:44–18:16	1	715	318			2.7	7.5	334	002
9/16	1169A	P-R buoy	17:45–18:20	2	1440	256	110	140	3.6	11.8	295	325
9/16	1169A	P-R buoy	17:45–18:20	2	1440	256	110	140	3.6	11.8	295	325
9/16	1169A	P-R buoy	17:45–18:20	2	1440	256	110	140	3.6	11.8	295	325
9/16	1169A	P-R buoy	17:45–18:20	2	1440	256	110	140	3.6	11.8	295	325
9/16	1169A	P-R buoy	17:45–18:20	2	1440	256	110	140	3.6	11.8	295	325
9/16	1169A	P-R buoy	17:45–18:20	2	1440	256	110	140	3.6	11.8	295	325
9/22	1255A	P-R buoy	18:03–18:38	2	935	177	094	124	2.7	8.3	243	273
9/22	1255A	P-R buoy	18:03–18:38	2	935	177	094	124	2.7	8.3	243	273
9/22	1255A	P-R buoy	18:03–18:38	2	935	177	094	124	2.7	8.3	243	273
9/22	1255A	P-R buoy	18:03–18:38	2	935	177	094	124	2.7	8.3	243	273
9/22	1255A	P-R buoy	18:03–18:38	2	935	177	094	124	2.7	8.3	243	273
9/22	1255A	CV-580 SAR (visual)	18:45-20:00	2	935	200	107	137				
9/22	1255A	CV-580 SAR (visual)	18:45-20:00	2	935	200	107	137				
9/22	1255A	CV-580 SAR (visual)	18:45-20:00	2	935	200	107	137				
9/22	1255A	CV-580 SAR (visual)	18:45-20:00	2	935	200	107	137				
9/22	1255A	CV-580 SAR (visual)	18:45-20:00	2	935	200	107	137				
9/23	1269A	P-R buoy	20:57–21:32	(Swiftsure Bank)		130*	102	132	2.5	5.1	090	120
9/23	1269A	CV-580 SAR (visual)	17:45–19:00	(Swiftsure Bank)		171*	099	129				
9/23	1269A	Tofino wave rider	18:00	(90 km northeast of Swiftsure Bank)		180†			1.6			
9/26	1306D	P-R buoy	07:57–08:32	(Swiftsure Bank)		245*	358	148	1.1	11.8	095	245
9/26	1306D	P-R buoy	07:57–08:32	(Swiftsure Bank)		130*	100	250	1.1	11.8	095	245
9/26	1306D	CV-580 SAR (visual)	07:25–08:25	(Swiftsure Bank)		Waves not discernible						
9/26	1306D	CV-580 SAR (visual)	07:25–08:25	(Swiftsure Bank)		Waves not discernible						
9/26	1306D	Tofino wave rider	08:00	(90 km northeast of Swiftsure Bank)		234†			0.94			

*A depth of 75 m was assumed for the wavelength computation. †A depth of 40 m was assumed at Tofino for the wavelength computation.

Table 3. Comparison of the Seasat and surface-aircraft data (Tables 1 and 2).

Date (1978)	Revolution	Space/time coincidence: Δx (km)	Space/time coincidence: Δt (hour/min)	λ: Δλ (m)	λ: Difference (%)	λ: Δθ_T (deg)
9/13	1126A	70	00:31	1	0.5	
9/13	1126A	90	00:31	24	12.4	
9/13	1126A	60	00:16	−51	−20.0	−13
9/13	1126A	60	00:16	9	3.5	18
9/13	1126A	25	00:16	−31	−12.1	01
9/13	1126A	25	00:16	3	1.2	−19
9/16	1169A	95	00:17	11	3.5	
9/16	1169A	25	00:18	4	1.6	−20
9/16	1169A	05	00:18	−25	−9.8	−27
9/16	1169A	25	00:18	−4	−1.6	−22
9/16	1169A	20	00:18	−41	−16.0	−19
9/16	1169A	70	00:18	33	12.9	−06
9/22	1255A	65	00:11	35	19.8	06
9/22	1255A	05	00:11	11	6.2	−06
9/22	1255A	00	00:11	5	2.8	−10
9/22	1255A	65	00:11	14	7.9	−03
9/22	1255A	100	00:11	4	2.3	−06
9/22	1255A	65	01:13	12	6.0	−07
9/22	1255A	05	01:13	−12	−6.0	−18
9/22	1255A	00	01:13	−18	−9.0	−23
9/22	1255A	65	01:13	−9	4.5	−16
9/22	1255A	100	01:13	−19	−9.5	−19
9/23	1269A	00	03:24	35	26.9	−11
9/23	1269A	00	00:14	−6	−3.5	−08
9/23	1269A					
9/26	1306D	00	00:15			
9/26	1306D	00	00.15			
9/26	1306D	00	00:05			
9/26	1306D	00	00:05			
9/26	1306D					

The practical consequence of the first observation is that the present data set is inadequate to address the important question of possible defocusing and resultant degradation (*8*) of Seasat SAR imagery of azimuth-traveling waves, for most waves were apparently traveling in a direction that was within 45° of the satellite range coordinate. This is so because the wave climatology during September for the region in the Gulf of Alaska corresponding to the imagery examined is such that most wave energy can be expected to propagate toward 90° (*9*) while the satellite heading at these latitudes was about 330°.

Despite these limitations on the data, some tentative conclusions can be drawn. There are 11 Seasat SAR/surface-aircraft data pairs in Table 3 which were acquired within 25 km and 1.5 hours of each other; this set yields agreement in wavelength to within about ± 15 percent and agreement in wave direction to within about ± 25°. Thus, the limited data set examined so far meets NOAA requirements for oceanographic measurement accuracy of ± 10 to ± 25 percent in wavelength and ± 10° to ± 30° in wave direction (*10*). If data pairs taken more than 25 km apart are included in the comparison, the agreement in wavelength is degraded to about ± 25 percent.

The data in Tables 1 and 2 also suggest a range of 1 to 2 m for $H_{1/3}$ where the lower limit for wave detection might fall. Thus, no waves were detected in Seasat SAR imagery acquired during revolution 1306, for which P-R buoy measurements indicated an $H_{1/3}$ of about 1 m; however, waves were detected during revolution 1126, for which an $H_{1/3}$ of about 2 m was observed. However, Tables 1 and 2 show that the dominant ocean wavelength and the relative angles between wind, wave, and satellite headings differed significantly in each case; these parameters may be equally as important as $H_{1/3}$ relative to wave detection capabilities. Thus caution must be exercised in the interpretation of this result.

Most of the GOASEX SAR data and surface measurements remain to be compared and analyzed. The preliminary nature of the data reduction, comparison, and analysis of the limited data set examined here should be noted. Seasat imagery of improved quality will be used in later analyses. The P-R buoy data will be processed at finer frequency resolution, and the resulting spectra transformed to wave number or wavelength space to improve comparisons with intensity spectra resulting from OFT's of Seasat imagery. Aircraft data will be digitized, so that geometric corrections and motion compensations can be made more accurately.

F. I. GONZALEZ
Pacific Marine Environmental Laboratory, National Oceanic and Atmospheric Administration, Seattle, Washington 98105
R. C. BEAL
Applied Physics Laboratory, Johns Hopkins University, Laurel, Maryland 20810
W. E. BROWN
Jet Propulsion Laboratory, California Institute of Technology, Pasadena 91103
P. S. DELEONIBUS, J. W. SHERMAN III
National Environmental Satellite Service, National Oceanic and Atmospheric Administration, Washington, D.C. 20233
J. F. R. GOWER
Institute of Ocean Sciences, Sidney, British Columbia, Canada V8L 4V2
D. LICHY
U.S. Army Corps of Engineers, Coastal Engineering Research Center, Fort Belvoir, Virginia 22060
D. B. ROSS
Sea-Air Interaction Laboratory, National Oceanic and Atmospheric Administration, Miami, Florida 33149
C. L. RUFENACH
Wave Propagation Laboratory, National Oceanic and Atmospheric Administration, Boulder, Colorado 80303
R. A. SHUCHMAN
Environmental Research Institute of Michigan, Ann Arbor 48107

References and Notes

1. W. E. Brown, Jr., C. Elachi, T. W. Thompson, *J. Geophys. Res.* **81**, 647 (1976); C. Elachi and W. E. Brown, *IEEE Trans. Antennas Propag.* **AP-25**, 84 (1977); T. R. Larson, L. I. Moskowitz, J. W. Wright, *ibid.* **AP-24**, 393 (1976); J. W. Wright, *ibid.* **AP-14**, 719 (1966); P. G. Teleki, R. A. Shuchman, W. E. Brown, Jr., W. McLeish, D. E. Ross, M. Mattie, *Proceedings of the Oceans '78 Conference* (Washington, D.C., 6 to 8 September 1978), pp. 639-648.
2. R. A. Shuchman, E. S. Kasischke, A. Klooster, *Synthetic Aperture Radar Ocean Wave Studies* (Final Report 131700-3-F, Environmental Research Institute of Michigan, Ann Arbor, 1978).
3. J. W. Goodman, *Introduction to Fourier Optics* (McGraw-Hill, New York, 1968).
4. G. H. Born, D. B. Lame, J. C. Wilkerson, Eds. "GOASEX Workshop Report" (Report 622-101, Jet Propulsion Laboratory, California Institute of Technology, Pasadena, 1979) (internal document), vol. 1, appendix A.
5. J. A. Ewing, *J. Mar Res.* **27**, 163 (1969); H. Mitsuyasu, F. Tasai, T. Suhara, S. Mizumo, L. Ohkusu, T. Honda, K. Rikiishi, *J Phys. Oceanog.* **5**, 750 (1975).
6. W. C. Chiu, *Am. J. Phys.* **35**, 642 (1967).
7. R. K. Raney, paper presented at the 5th Canadian Remote Sensing Symposium, Victoria, British Columbia, 1978.
8. R. A. Shuchman and J. S. Zelenka, *Boundary-Layer Meteorol.* **13**, 181 (1978); A. Jain, *J. Appl. Phys.* **15**, 323 (1973).
9. U.S. Navy, *U.S. Navy Marine Climatic Atlas of the World*, vol. 2, *North Pacific Ocean* (Naval Air Force Document 50-1C-529, Naval Weather Service Detachment, Asheville, N.C., 1977), p. 265.
10. "NOAA Program Development Plan for Seasat-A: Research and Applications" (Report NOAA-S/T 77-2574, Department of Commerce, Washington, D.C., March 1977), p. 1-2.
11. We thank J. C. Dwyer of the Environmental Research Institute of Michigan (ERIM) and T. Bicknell of the Jet Propulsion Laboratory for providing the optical Fourier transforms. We thank P. G. Teleki and J. Dunne for their advice and helpful comments during and after the GOASEX Workshop. The ERIM portion of the analysis was supported under NOAA National Environmental Satellite Service contract MO-AO1-78-00-4339. Portions of the research described in this report were carried out by the Jet Propulsion Laboratory, California Institute of Technology, and were sponsored by the National Oceanic and Atmospheric Administration and National Aeronautics and Space Administration.

20 April 1979

Seasat Visible and Infrared Radiometer

Abstract. *Visual and infrared images produced by the Seasat visible and infrared radiometer (VIRR) are adequate for the identification of cloud, land, and water features. A statistical comparison of VIRR-derived sea-surface temperatures in a cloud-free region with a National Oceanic and Atmospheric Administration analysis based on various surface measurements taken in the same region showed agreement to ± 1.7°K root-mean-square.*

The visible and infrared radiometer (VIRR), a supporting instrument system on Seasat, has as its principal function to provide images of visual reflection and thermal infrared emission from ocean, coastal, and atmospheric features that can aid in interpreting the data from the other Seasat sensors. The VIRR is also expected to provide some derived quantitative measurements of such factors as sea-surface temperature and cloud-top height.

All the instruments on-board Seasat except the VIRR are microwave systems, active or passive, but only one other instrument in addition to the VIRR, the synthetic aperture radar (SAR), is an imaging system. The VIRR will provide images encompassing the data swaths of all the other Seasat sensors, with a ground resolution equal to or greater than that of any other Seasat sensor except the SAR and the radar altimeter. Thus, investigators can determine whether the field of view of their instrument is partly or completely filled by cloud, determine something about the cloud type and height, confirm the presence or absence of land, and possibly detect ocean thermal fronts.

0036-8075/79/0629-1421$00.50/0